Inorganic Chemistry

ARTICLE

pubs.acs.org/IC

Synthesis and Crystal Structure of a Pr_5Ni_{19} Superlattice Alloy and Its Hydrogen Absorption−Desorption Property

Kenji Iwase,*[,†] Kouji Sakaki,[‡] Junko Matsuda,[‡] Yumiko Nakamura,[‡] Toru Ishigaki,[†] and Etsuo Akiba[‡]

[†]Frontier Research Center for Applied Sciences, Ibaraki University, 162-1 Shirakata, Tokai, Naka, Ibaraki 319-1106, Japan

[‡]National Institute of Advanced Industrial Science and Technology (AIST), AIST Central-5, 1-1-1 Higashi, Tsukuba, Ibaraki 305-8565, Japan

ABSTRACT: The intermetallic compound Pr_5Ni_{19}, which is not shown in the Pr−Ni binary phase diagram, was synthesized, and the crystal structure was investigated by X-ray diffraction (XRD) and transmission electron microscopy (TEM). Two superlattice reflections with the Sm_5Co_{19}-type structure (002 and 004) and the Pr_5Co_{19}-type structure (003 and 006) were observed in the 2θ region between 2° and 15° in the XRD pattern using Cu Kα radiation. Rietveld refinement provided the goodness-of-fit parameter S = 6.7 for the Pr_5Co_{19}-type (3R) structure model and S = 1.7 for the Sm_5Co_{19}-type (2H) structure model, indicating that the synthesized compound has a Sm_5Co_{19} structure. The refined lattice parameters were a = 0.50010(9) nm and c = 3.2420(4) nm. The high-resolution TEM image also clearly revealed that the crystal structure of Pr_5Ni_{19} is of the Sm_5Co_{19} type, which agrees with the results from Rietveld refinement of the XRD data. The $P-C$ isotherm of Pr_5Ni_{19} in the first absorption was clearly different from that in the first desorption. A single plateau in absorption and three plateaus in desorption were observed. The maximum hydrogen storage capacity of the first cycle reached 1.1 H/M, and that of the second cycle was 0.8 H/M. The 0.3 H/M of hydrogen remained in the metal lattice after the first desorption process.

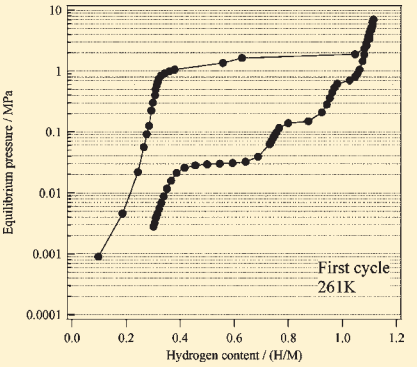

1. INTRODUCTION

The hydrogen absorption property and structural change observed upon hydrogenation of the intermetallic compounds Laves-type RNi_2 (R = Y, La, Ce, Pr, Nd, Sm, Gd, Tb, Dy, Ho, Er) and $CaCu_5$-type RNi_5 (R = La, Ce, Pr, Nd, Sm) have been extensively investigated.[1−4] The RNi_2 Laves phase becomes amorphous after hydrogenation at 323 K[1] except for $NdNi_2$, which decomposes into NdH_2 and $NdNi_5$.[1] $P-C$ isotherms of RNi_5 measured up to 35 MPa in the temperature range between 196 and 423 K have been reported.[3] $LaNi_5$ and $CeNi_5$ show a single plateau, but two plateaus have been observed for $PrNi_5$, $NdNi_5$, and $SmNi_5$.

RNi_3 and R_2Ni_7 (R = La, Ce, Pr, Nd, Sm, Gd, Tb, Dy, Ho, Y, Er) exist as intermetallic compounds with superlattice structures.[5] They consist of cells with $MgZn_2$- and $CaCu_5$-type structures stacked along the c axis in ratios of 1:1 and 1:2. RNi_3 (R = La, Pr, Nd, Gd, Y, Er, Tb, Dy, Ho, Tm, Yb, Pu) shows a rhombohedral $PuNi_3$-type structure with lattice parameters of a = 0.4913−0.5086 nm and c = 2.416−2.501 nm, while $CeNi_3$ has a hexagonal $CeNi_3$-type structure with a = 0.496 nm and c = 1.656 nm. R_2Ni_7 compounds exhibit two types of crystal structures: a hexagonal Ce_2Ni_7-type structure (R = La, Ce, Pr, Nd, Sm, Gd, Tb, Dy) with a = 0.4941−0.5083 nm and c = 2.425−2.509 nm or a rhombohedral Gd_2Co_7-type structure (R = La, Pr, Nd, Sm, Gd, Tb, Dy, Ho, Y, Er) with a = 0.4928−0.5056 nm and c = 3.607−3.698 nm.[5] Some compounds such as La_2Ni_7 have polymorphs, whose stability depends on the temperature.[6] Detailed investigations on the hydrogen absorption properties of these R_2Ni_7 compounds, excluding La_2Ni_7[7] and Ce_2Ni_7,[8] have not yet been reported.

There have only been a few reports on R_5Ni_{19}-type compounds. Yamamoto et al. studied the crystal structure of intermetallic compounds in the La−Ni system using transmission electron microscopy (TEM) and found La_5Ni_{19} with a Pr_5Co_{19}-type structure for the first time.[9] The Pr_5Co_{19}-type (3R) structure has three blocks along the c axis; each block is composed of one layer of $MgZn_2$-type cells and three layers of $CaCu_5$-type cells. The phase is stable only in a narrow temperature range around 1273 K. The hydrogenation property of this phase is not clear because the reported $P-C$ isotherm was measured for a multiphase sample containing both La_5Ni_{19} and $LaNi_5$. Takeda et al. reported the crystal structures of Sm_5Ni_{19}.[10] The sample was annealed at 1173 K for 1 week inside an argon-sealed silica tube. Six superlattice structures (2H, 3R, 4H, 6H, 9R, and 12R) were found by TEM. No reliable $P-C$ isotherm for R_5Ni_{19} binary compounds has been reported.

The phase diagram of the Pr−Ni system shows seven phases in the equilibrium state: Pr_3Ni_1, Pr_7Ni_3, PrNi, $PrNi_2$, $PrNi_3$, Pr_2Ni_7, and $PrNi_5$.[11] Pr_2Ni_7 has two types of crystal structures: a hexagonal Ce_2Ni_7-type structure at high temperature and a rhombohedral Gd_2Co_7-type structure at low temperature. Its phase stability for temperature is opposite to that observed in La_2Ni_7. Pr_5Ni_{19} is not shown in the Pr−Ni binary phase diagram. Recently, the synthesis of Pr_5Ni_{19} has been reported,[12] but the synthesis conditions, structure, and hydrogenation properties have not been fully elucidated.

Received: February 6, 2011
Published: April 18, 2011

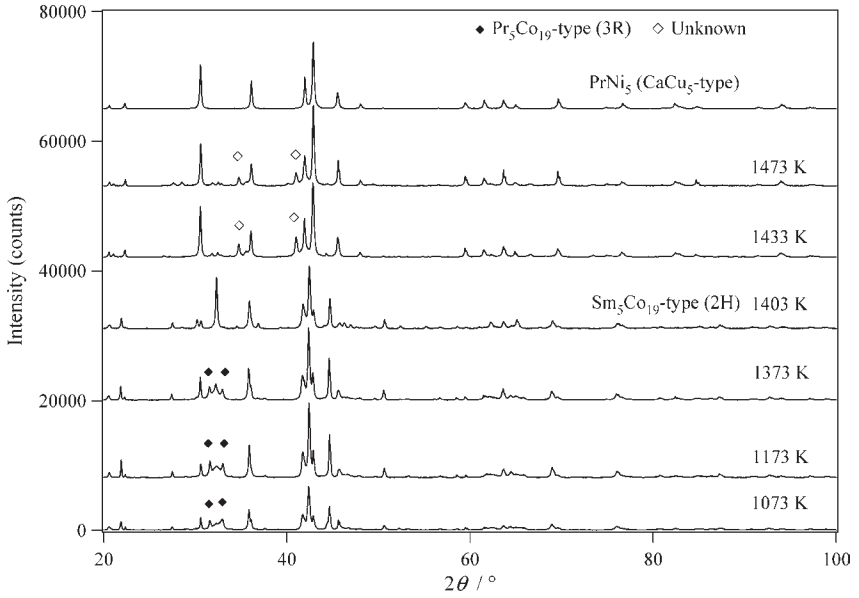

Figure 1. XRD profiles of the Pr_5Ni_{19} alloy annealed and quenched at several temperatures. The data of the $PrNi_5$ alloy annealed at 1323 K for 10 h are also shown for reference.

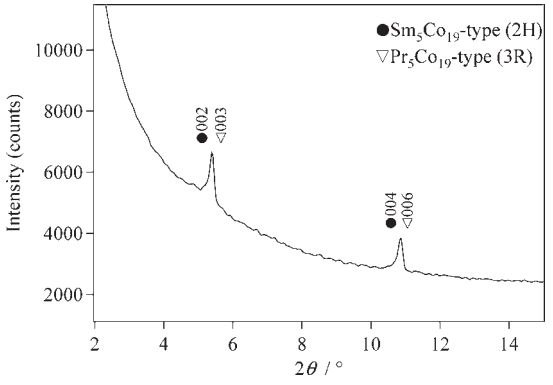

Figure 2. XRD pattern for Pr_5Ni_{19} in a low-angle region. Two superlattice peaks, which may be for Sm_5Co_{19}- or Pr_5Co_{19}-type structures, were clearly observed.

This study focused on the crystal structure and hydrogen absorption−desorption properties of Pr_5Ni_{19}. We attempted to synthesize the Pr_5Ni_{19} compound and to understand the crystal structure and hydrogen absorption property by using X-ray diffraction (XRD), TEM, and $P-C$ isotherm measurements. The synthesis temperature and crystal structure were compared with those reported for La_5Ni_{19}. The absorption and desorption properties are discussed by referring to the properties reported for related compounds with superstructures.

2. EXPERIMENTAL SECTION

A Pr−Ni binary alloy was prepared by arc-melting Pr and Ni metals (99.9%) in an argon atmosphere. The Pr_5Ni_{19} ingot was annealed in the temperature region between 1073 and 1473 K under a vacuum and quenched in ice water. The XRD profiles of the quenched samples are shown in Figure 1. The single phase was successfully synthesized when it was annealed at 1403 K followed by quenching. The $CaCu_5$-type and unknown structures increased and the Sm_5Co_{19}-type structure disappeared when the temperature rose over 1433 K. The Pr_5Co_{19}- and Sm_5Co_{19}-type

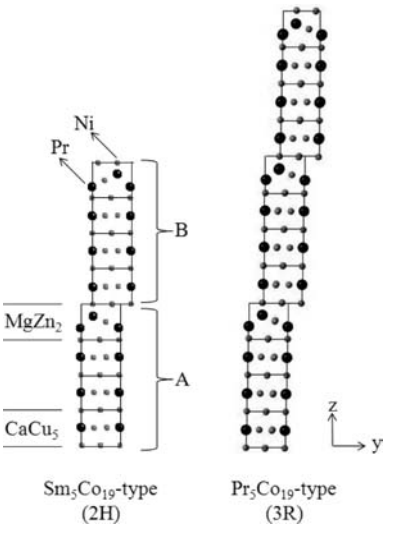

Figure 3. Sm_5Co_{19}-type (2H) and Pr_5Co_{19}-type (3R) crystal structures.

structures coexisted in the temperature region between 1073 and 1373 K. Finally, the Pr_5Ni_{19} sample was obtained by annealing at 1403 K for 20 h under a vacuum of 2.0×10^{-4} Pa and quenching in ice water.

The powder sample was sieved to a particle size of <20 μm for XRD measurements. The XRD data were collected on a Rigaku RINT-2500 V diffractometer. Cu Kα radiation monochromatized with a curved graphite diffractometer was used in a step-scan mode. The structural parameters were refined with the Rietveld refinement program RIETAN-2000.[13−15] The reliability of the fitting was judged from the "goodness-of-fit" S; this was defined as $S = R_{wp}/R_e$, where R_{wp} is a residue of the weighted pattern and R_e is the statistically expected residue. A JEOL JEM-2100F transmission electron microscope operating at 200 kV was used in the TEM observations.

The sample for the $P-C$ isotherm measurement was sealed in a stainless steel container, heated in a vacuum at 393 K for 1 h, and then

dx.doi.org/10.1021/ic200253w |Inorg. Chem. 2011, 50, 4548–4552

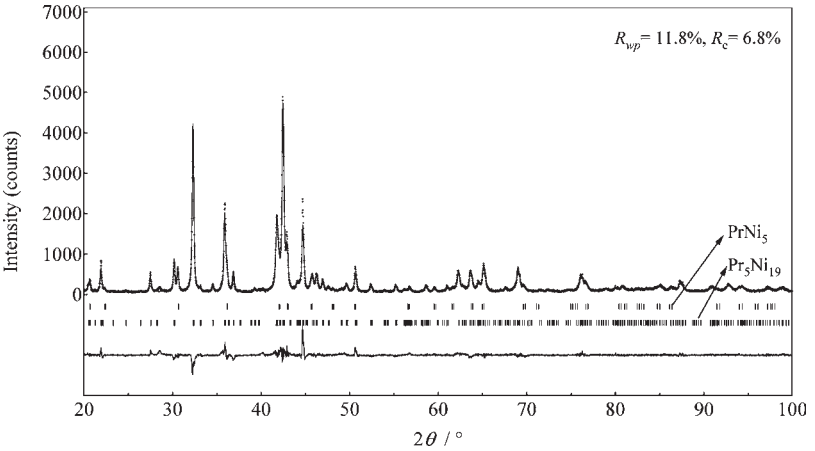

Figure 4. Rietveld refinement of XRD data for the Pr_5Ni_{19} sample. A model containing Sm_5Co_{19}-type Pr_5Ni_{19} and $CaCu_5$-type $PrNi_5$ was applied. The line indicates calculated intensities, and the points superimposed on it are the observed intensities. The tick marks below the pattern indicate the position of the allowed Bragg reflections for $PrNi_5$ (upper) and Pr_5Ni_{19} (lower). The bottom curve is the difference between the observed and calculated intensities.

evacuated at 261 K for 1 h. The *P*−*C* isotherm was measured using Sieverts' method with no other pretreatment for activation. Before the second cycle measurement, the sample was evacuated at 261 K for 3 h.

3. RESULTS

3-1. Crystal Structure of Pr_5Ni_{19}. The XRD profile of Pr_5Ni_{19} in the 2θ region between 2° and 15° is shown in Figure 2. Two superlattice reflections of the Sm_5Co_{19}-type structure (002 and 004) or Pr_5Co_{19}-type structure (003 and 006) were clearly observed. Sm_5Co_{19}-type (2H) and Pr_5Co_{19}-type (3R) crystal structures are shown in Figure 3. The observed reflections corresponded to d = 1.62 and 0.81 nm. The XRD pattern also indicated that no Pr−Ni binary alloy with other superstructures ($PuNi_3$-, Gd_2Co_7-, or Ce_2Ni_7-type structures) was contained in the sample.

The structural parameters of Pr_5Ni_{19} were determined by Rietveld refinement of the XRD data in the 2θ region between 20° and 100°. An initial structural model based on the Pr_5Co_{19}-type structure (space group $R\bar{3}m$), the same as La_5Ni_{19}, was adopted. The calculated pattern did not fit well with the observed pattern. The goodness-of-fit S was 6.7. We then used another model of the Sm_5Co_{19}-type structure (space group $P6_3/mmc$); this one agreed fairly well with the observed data. In order to obtain a better fit, we carried out refinement with a two-phase model containing Sm_5Co_{19}-type Pr_5Ni_{19} and $CaCu_5$-type $PrNi_5$. Figure 4 shows the refined pattern with the two-phase model, and the calculated pattern fit better with the observed pattern. The value of S was 1.7, and the mass fractions of Pr_5Ni_{19} and $PrNi_5$ were 90% and 10%, respectively. The refined lattice parameters of Pr_5Ni_{19} were a = 0.50010(9) nm and c = 3.2420(4) nm.

3-2. TEM Analysis of Pr_5Ni_{19}. The selected-area electron diffraction (SAED) pattern taken along the ⟨010⟩ direction of Pr_5Ni_{19} is shown in Figure 5a. The SAED pattern was consistently indexed as the Sm_5Co_{19}-type structure. The 008 and 100 spots were clearly observed. The high-resolution TEM (HRTEM) image of Pr_5Ni_{19} viewed along [010] is shown in Figure 5a. Four bright spots indicating Pr atoms were observed in the c-axis direction. The Sm_5Co_{19}-type (2H) structure has two units (A and B units) along the c axis, as shown in Figure 3; each unit is composed of one layer of $MgZn_2$-type cells and three layers of $CaCu_5$-type cells. This agreed well with the HRTEM image. A Pr_5Co_{19}-type (3R) structure was not observed in the HRTEM image. An SAED pattern taken along ⟨001⟩ and a HRTEM image viewed along [001] are shown in Figure 5b.

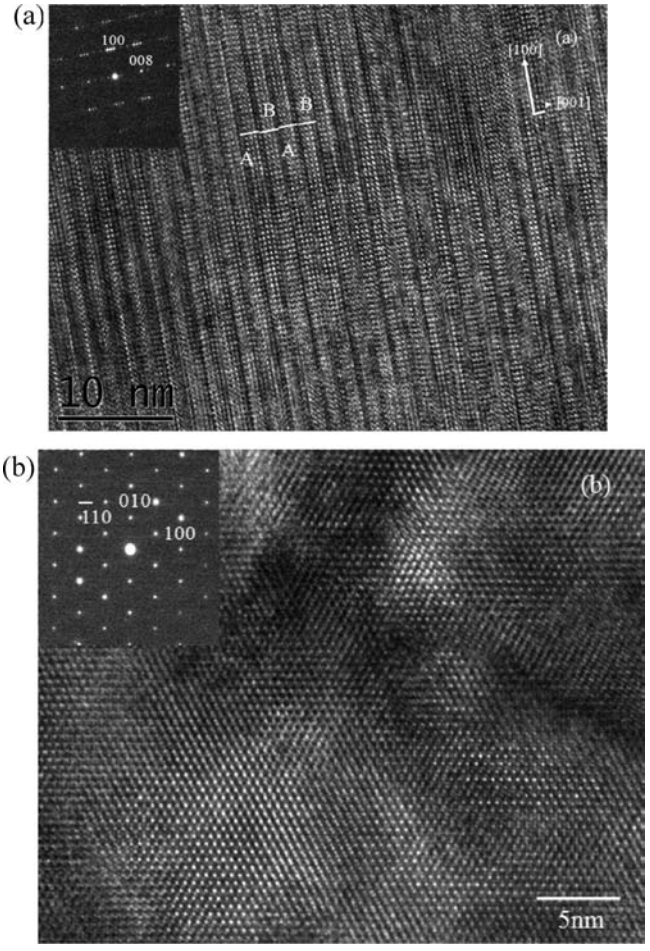

Figure 5. HRTEM images and an SAED pattern of Pr_5Ni_{19}: incidence of (a) [010] for HRTEM and ⟨010⟩ for SAED and (b) [001] for HRTEM and ⟨001⟩ for SAED.

dx.doi.org/10.1021/ic200253w |*Inorg. Chem.* 2011, 50, 4548–4552

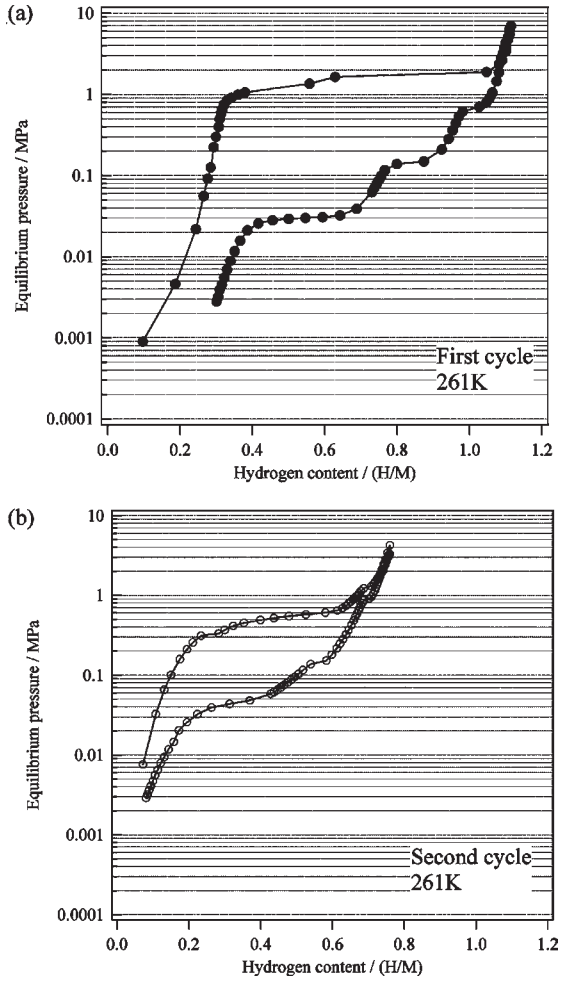

Figure 6. $P-C$ isotherm of Pr_5Ni_{19} at 261 K: (a) first absorption−desorption; (b) second absorption−desorption.

The −110, 010, and 100 spots were clearly observed. These results revealed that Pr_5Ni_{19} has a Sm_5Co_{19}-type crystal structure, which is consistent with the XRD results.

3-3. $P-C$ Isotherm of Pr_5Ni_{19}. The $P-C$ isotherm of Pr_5Ni_{19} for the first absorption and desorption process at 261 K is shown in Figure 6a. The $P-C$ isotherm of absorption was clearly different from that of desorption. In the absorption process, the hydrogen content increased gradually up to 0.3 H/M and showed a plateau between 0.3 and 1.0 H/M. The plateau pressure was approximately 1.6 MPa. The maximum hydrogen capacity reached 1.1 H/M at 7.0 MPa. However, in the desorption process, three plateaus were clearly observed; these had desorption pressures of 0.7, 0.14, and 0.03 MPa. The width of the plateau region increased with decreasing desorption pressure. Figure 6b shows the $P-C$ isotherm of the second absorption and desorption at 261 K. The maximum hydrogen capacity reached 0.8 H/M. The absorption plateau pressure was approximately 0.5 MPa. After the first full desorption down to 0.003 MPa, 0.3 H/M of hydrogen remained in the sample.

4. DISCUSSION

4-1. Crystal Structure. Buschow and Van Der Goot reported that $PrNi_3$ has a rhombohedral $PuNi_3$-type structure[5] according to their XRD results. The lattice parameters were a = 0.5035 nm and c = 2.482 nm. Pr_2Ni_7 has a rhombohedral Gd_2Co_7-type structure with lattice parameters of a = 0.5015 nm and c = 3.664 nm[5] at room temperature and a hexagonal Ce_2Ni_7-type structure with a = 0.5015 nm and c = 2.444 nm[5] at high temperature. In this study, we successfully synthesized the Pr_5Ni_{19} phase and revealed that the crystal structure is of the Sm_5Co_{19} type (2H) with lattice parameters of a = 0.50010(9) nm and c = 3.2420(4) nm. A Pr_5Co_{19}-type (3R) structure was not observed in either the XRD profile or the HRTEM image. The dimensions of the $PrNi_5$ cells (a = 0.5001 nm and c = 0.3828 nm) in Pr_5Ni_{19} were quite different from those of the $PrNi_5$ compound (a = 0.4964 nm and c = 0.3977 nm). Hydrogen occupation is often based on the interstitial size and distance between two sites. $PrNi_5$ cells in the Pr_5Ni_{19} alloy should show a hydrogen occupation different from that of the $PrNi_5$ alloy. When the lattice parameters were compared for $PrNi_3$, Pr_2Ni_7, and Pr_5Ni_{19}, a decreased with the ratio of $PrNi_5$ cells to Pr_2Ni_4 cells and was closer to that for the $PrNi_5$ compound.

Lemort et al. recently reported the synthesis of Pr_5Ni_{19}.[12] The sample was annealed at 1373 K for 35 days in a silica tube under a vacuum before quenching to room temperature. They reported that the sample contained Sm_5Co_{19}-type, Pr_5Co_{19}-type, and $CaCu_5$-type structures after Rietveld refinement of the XRD pattern; these structures had mass fractions of 56%, 37%, and 7%, respectively. The difference curve of the Rietveld refinement also suggests the existence of another phase. Our results indicated that the Pr_5Co_{19}- and Sm_5Co_{19}-type structures coexisted in the temperature region between 1073 and 1373 K and that Pr_5Ni_{19} with the Sm_5Co_{19}-type structure is only stable in a narrow temperature area around 1403 K. Lemort et al. also reported $P-C$ isotherms; compared to our results, the maximum hydrogen capacities were similar, but the shapes of the curves were different. This is probably because of the differences in the contained phases and activation processes.

Three compounds with superlattice structures have been reported for the La−Ni binary system. Yamamoto et al. reported a TEM study showing that La_5Ni_{19} has a rhombohedral Pr_5Co_{19}-type (3R) structure around 1273 K.[9] This phase is stable at around 1273 K but decomposes into La_2Ni_7 and $LaNi_5$ phases below 1173 K.

Buschow and Van Der Goot reported that La_2Ni_7 has a hexagonal Ce_2Ni_7-type structure at 873 K and a rhombohedral Gd_2Co_7-type structure that is stable at temperatures close the melting temperature.[6] They also reported that $LaNi_3$ has a rhombohedral $PuNi_3$-type structure. On the other hand, in the Pr−Ni system, Pr_5Ni_{19} is a hexagonal Sm_5Co_{19}-type structure, as indicated above. Pr_2Ni_7 has a rhombohedral Gd_2Co_7-type structure at room temperature and a hexagonal Ce_2Ni_7-type structure at 1223 K.[5] $PrNi_3$ has a rhombohedral $PuNi_3$-type structure like $LaNi_3$. The stability of polymorphous phases for each stoichiometry is partly different between the La−Ni and Pr−Ni binary systems.

4-2. Phase Transformation during the Hydrogen Absorption−Desorption Process. The $P-C$ isotherm of Pr_5Ni_{19} for the first cycle (Figure 6a) clearly showed a single plateau in absorption and three plateaus in desorption. From the Rietveld refinement shown in Figure 4, the mass fractions of Pr_5Ni_{19} and $PrNi_5$ were 90% and 10%, respectively. The refined lattice parameters of $PrNi_5$, i.e., a = 0.4967(1) nm and c = 0.39733(7) nm, agreed with those of a = 0.49659(2) nm and c = 0.39766(2) nm reported by Senoh et al.[3] They reported $P-C$

dx.doi.org/10.1021/ic200253w |Inorg. Chem. 2011, 50, 4548–4552

isotherms up to 35 MPa and a van't Hoff plot of $PrNi_5$. Two plateaus were clearly observed between 248 and 323 K. From the van't Hoff plot, the higher and lower desorption plateau pressures were calculated to be 1.0 and 0.22 MPa at 261 K. In contrast, the desorption pressures of three plateaus for the Pr_5Ni_{19} sample containing $PrNi_5$ were 0.7, 0.14, and 0.03 MPa in this study. The plateau pressures of our results do not agree with those of single-phase $PrNi_5$.[3] This indicates that the obtained $P-C$ isotherm is barely affected by $PrNi_5$. There are two possible distributions of hydrogen in the cells comprising the superlattice structures: most of the H atoms occupy the Pr_2Ni_4 cell like in $La_2Ni_7D_{6.5}$,[16] or the H atoms occupy both Pr_2Ni_4 and $PrNi_5$ cells evenly like in $La_4MgNi_{19}D_{26}$.[17] This can be elucidated from the expansion of each cell using in situ XRD as well as from refinement of the occupancy of each hydrogen site using in situ neutron diffraction. In our previous study of La_2Ni_7,[7] the $P-C$ isotherm showed only one clear plateau. The results of in situ XRD along the $P-C$ isotherm indicated that hydrogen is absorbed in La_2Ni_4 cells first before entering the plateau region; it is then also absorbed in the $LaNi_5$ cells in the plateau region. In desorption, hydrogen is desorbed mostly from the $LaNi_5$ cells, and around 0.7 H/M of hydrogen remains in the La_2Ni_4 cells. In Pr_5Ni_{19}, the $P-C$ isotherm suggests that hydrogen corresponding to about 20% of the capacity may be absorbed in the Pr_2Ni_4 cell before entering the plateau, and in the plateau region, the rest of the hydrogen is absorbed in the Pr_2Ni_4 and $PrNi_5$ cells simultaneously. However, in desorption, hydrogen is desorbed stepwise, e.g., from one type of cell to another, or part by part. We plan to study the phase transformation and hydrogen occupation of Pr_5Ni_{19} during absorption and desorption by using in situ XRD and neutron diffraction.

5. CONCLUSIONS

We successfully synthesized the compound Pr_5Ni_{19} and investigated the crystal structure and hydrogenation properties. The crystal structure of Pr_5Ni_{19} was revealed to be of the hexagonal Sm_5Co_{19} type by Rietveld refinement of XRD data and HRTEM observations.

The $P-C$ isotherm of Pr_5Ni_{19} showed a single plateau in absorption but three plateaus in desorption. This suggests that hydrogen is absorbed in all hydrogen sites simultaneously but desorbed from part by part. The maximum hydrogen capacity was 1.1 H/M, and 0.3 H/M of the hydrogen remained after the first desorption.

AUTHOR INFORMATION

Corresponding Author

*E-mail: fbiwase@mx.ibaraki.ac.jp. Tel: +81-29-352-3233. Fax: +81-29-287-7189.

ACKNOWLEDGMENT

We thank Dr. H. Enoki (AIST), Dr. K. Asano (AIST), and Dr. K. Mori (Kyoto University) for their helpful advice.

REFERENCES

(1) Aoki, K.; Yamamoto, T.; Masumoto, T. *Scr. Metall.* **1987**, *21*, 27–31.

(2) Nomura, K.; Uruno, H.; Ono, S. *J. Less-Common Met.* **1985**, *107*, 221–230.

(3) Senoh, H.; Takeichi, N.; Takeshita, H.; Tanaka, H.; Kiyobayashi, T.; Kuriyama, N. *Mater. Trans.* **2003**, *44*, 1663–1666.

(4) Senoh, H.; Takeichi, N.; Kuriyama, N. *Mater. Trans.* **2004**, *45*, 2610–2613.

(5) Buschow, K. H. J.; Van Der Goot, A. S. *J. Less-Common Met.* **1970**, *22*, 419–428.

(6) Virkar, A. V.; Raman, A. *J. Less-Common Met.* **1968**, *18*, 59–66.

(7) Iwase, K.; Sakaki, K.; Nakamura, Y.; Akiba, E. *Inorg. Chem.* **2010**, *49*, 8763–8768.

(8) Denys, R. V.; Yartys, V. A.; Sato, M.; Riabov, A. B.; Delaplane, R. G. *J. Solid State Chem.* **2007**, *180*, 2566–2576.

(9) Yamamoto, T.; Inui, H.; Yamaguchi, M.; Sato, K.; Fujitani, S.; Yonezu, I.; Nishio, K. *Acta Mater.* **1997**, *45*, 5213–5221.

(10) Takeda, S.; Kitano, Y.; Komura, Y. *J. Less-Common Met.* **1982**, *84*, 317–325.

(11) *Binary Alloy Phase Diagrams*, 2nd ed. plus updates; Okamoto, H., Ed.; ASM International: Materials Park, OH, 1996.

(12) Lemort, L.; Latroche, M.; Knosp, B.; Bernard, P. *J. Alloys Compd.* **2011**in press.

(13) Izumi, F. http://homepage.mac.com/fujioizumi/.

(14) Izumi, F. *Rigaku J.* **2000**, *17* (1), 34–45.

(15) Izumi, F.; Young, R. A. *The Rietveld Method*; International Union of Crystallography: Oxford University Press: Oxford, U.K., 1993; p 13.

(16) Yartys, V. A.; Riabov, A. B.; Denys, R. V.; Sato, M.; Delaplane, R. G. *J. Alloys Compd.* **2007**, *408–412*, 273–279.

(17) Nakamura, J.; Iwase, K.; Hayakawa, H.; Nakamura, Y.; Akiba, E. *J. Phys. Chem.* **2009**, *113*, 5853–5859.